Multivalency Pattern Recognition to Sort Colloidal Assemblies

*Sebastian Loescher and Andreas Walther**

Multivalent interaction is an important principle for self-assembly and has been widely used to assemble colloids. However, surface binding partners are statistically distributed, which falls short of the interaction possibilities arising from geometrically controlled multivalency patterns as seen in viruses. Herein, the precision provided by 3D DNA origami is exploited to introduce multivalency pattern recognition via designing geometrically precise interaction patterns at patches of patchy nanocylinders. This gives rise to self-sorting of colloidal assemblies despite having the same type and number of supramolecular binding motifs—solely based on the pattern located on a 20×20 nm^2 cross-section. The degree of sorting can be modulated by the geometric overlap of patterns and homo; mixed and alternating supracolloidal polymerizations are demonstrated. Multivalency patterns are able to provide an additional information layer to organize soft matter, important towards engineering of biological responses and functional materials design.

Multivalent interactions in nature guide structure formation, and amplify binding specificity and binding strength via molecular recognition of interaction patterns.[1] In this regard, especially the geometric control to spatially organize multivalent patterns together with control over rigidity and spacing is important, which influences, for instance, virus uptake in cells and immunoresponse.[2] In synthetic systems, such multivalent

S. Loescher, Prof. A. Walther[+]
Institute for Macromolecular Chemistry
University of Freiburg
Stefan-Meier-Strasse 31, 79104 Freiburg, Germany
E-mail: andreas.walther@uni-mainz.de
S. Loescher, Prof. A. Walther
Freiburg Materials Research Center
University of Freiburg
Stefan-Meier-Strasse 21, 79104 Freiburg, Germany
S. Loescher, Prof. A. Walther
Freiburg Center for Interactive Materials and Bioinspired Technologies
(FIT)
University of Freiburg
Georges-Köhler-Allee 105, 79110 Freiburg, Germany

The ORCID identification number(s) for the author(s) of this article can be found under https://doi.org/10.1002/smll.202005668.

[+]Present address: Department of Chemistry, Duesbergeweg 10-14, University of Mainz, 79104 Mainz, Germany

pattern recognitions have been investigated for ligand arrangements on phage capsids nanoparticles (NPs) targeting influenza viruses[3] or in DNA origami templates for arrangement of immunogens for B-cell activation.[4] In DNA nanotechnology, pattern recognition of base-stacking interactions for connecting 2D DNA origami sheets at the edges was demonstrated by Rothemund and co-workers,[5] but the concept has not been transduced to particulate assemblies.

In the colloid and NP assembly field, multivalent interactions are commonly used to organize lattice structures of isotropic particles.[6] Different superstructures beyond simple lattices have been realized using patchy colloi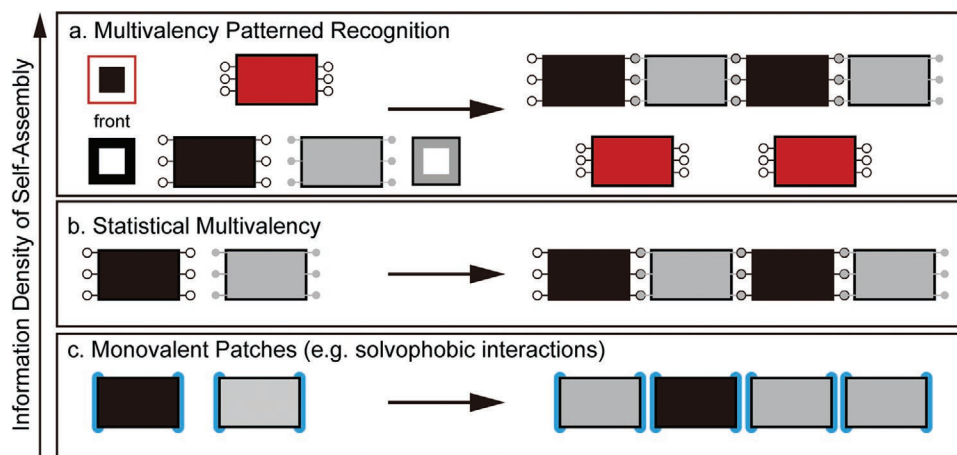ds with anisotropic interactions.[7] Yet, the arrangement of multivalent binding partners in such systems is purely statistical (**Scheme 1**b), and supracolloidal particulate assemblies that employ supramolecular binding have to the best of our knowledge not explored the possibilities of multivalency patterns to control structure formation and sorting events, even more in multicomponent systems. Although various approaches can be used to prepare patchy NPs,[7b,8] the highest precision is currently available by DNA origami,[9] and to some extent by engineered proteins.[10] 3D DNA origami has been employed to prepare complex plasmonic nanostructures,[11] enzyme complexes,[12] and tools for single molecule investigations.[13] Hierarchical SA of 3D DNA origami NPs to create discrete or fibrillar superstructures relies mainly on DNA interactions such as base-pairing[14] or shape-complementary base-stacking interactions.[15] Recently, we introduced host/guest complexation to 3D DNA origami NPs as non-DNA interaction for higher level SA, making use of strong multivalency effects,[16] and others have reported the use of coiled-coil peptide motifs.[17]

We hypothesized that the precise geometric arrangement of interacting groups as multivalency patterns on 3D DNA origami NPs would impart new possibilities for controlled and highly selective interactions in NP SA, going beyond the possibilities of spatially uncontrolled multivalent interactions in common NPs with statistically distributed binding partners (Scheme 1). For instance, geometrically arranged multivalency patterns could provide opportunities for controlled co-assembly or self-sorting of mixtures of NPs using i) the same interaction chemistry, and ii) the same amount of interacting groups, yet (iii) at spatially varied positions on the patch. Indeed, here, we demonstrate geometric multivalency pattern recognition in systems containing two 3D DNA origami NPs that are equipped

Scheme 1. Interactions in patchy NP SA. a) Multivalency pattern recognition of designed patterns. b) Statistical distribution of multivalent interactions at patches enhances binding strength. c) Assembly of NPs without specific multivalent interactions (e.g., solvophobic interactions) leads to simple association without control over binding strength or recognition.

at their front and back side (patches) with different multivalency patterns based on β–-cyclodextrin/adamantane host/guest interactions. We demonstrate that by variation of pattern overlaps, 3D DNA origami NPs either self-sort into pure homo-fibrils, mixed/blocky hetero-fibrils, or alternating fibrils. Thus, the introduction of pattern recognition is shown to offer another control layer to encode information in colloidal SA.

We prepared two different cylindrical origamis that allow for an orthogonal functionalization of both tips/patches with precise multivalency patterns in a Janus configuration (**Figure 1**a).[8] Both origami have different sizes to distinguish them in transmission electron microscopy (TEM): i) Origami A: a 72 helix cuboid (blue, m13mp18 scaffold) with 40 nm length (cross-section $\approx 24 \times 18$ nm), and ii) origami B: a 50 helix cuboid (orange, p8064 scaffold) with 60 nm length (cross-section $\approx 20 \times 16$ nm) (Figure 1b). The docking strand patterns at the two origami tips can be functionalized selectively at the individual DNA helices of the hexagonal lattice by complimentary Adamantane (Adm, guest) or β-cyclodextrin (βCD, host)-bearing ssDNA. In a typical experiment both origami are present in equimolar ratio in a solution (10 nm each) and a mixture of ssDNA-host/guest strands is added to initiate supracolloidal fibrillization by quick hybridization to the tips of the origami and subsequent supracolloidal assembly (Figure 1c).

To understand the possibility of self-sorting self-assembly (SA) versus mixed co-assembly of the two 3D DNA origami NPs, we

designed 3 different multivalency patterns of 12 βCD/Adm units on the large cross-section of origami A (**Figure 2**a). The small cross-section of origami B was patterned with a closed packed design (B1) also containing 12 host/guest pairs. Each origami carries host entities on one side and guest entities on the other allowing for homo-assembly or for hetero/co-assembly. Origami A1 and B1 exhibit non-complementary patterns in a perfect aligned arrangement (termed: 0% pattern overlap). A small number of interactions are only possible if the origami A1–B1 bind in rotation (i.e., 3 binding partners). Origami A2 and B1 possess a maximum of 6 geometrically fitting overlaps (50% pattern overlap). Origami A3 and B1 have a full match (100% pattern overlap).

Supracolloidal copolymerization is initiated once host/guest strands are added to a solution containing both origami, and fibril distributions were evaluated after 48 h using ex-situ TEM analysis (Figure 2c). The origami A (blue) and B (orange) are color-coded for better visualization. We evaluated the composition of fibrils with a degree of polymerization (DP) of DP > 8 and identified the number fraction of homo-repeats (Figure 2b). Focusing on a DP > 8 minimizes end group and oligomer effects, because oligomers have a low statistical chance for crossovers. The dot area in the dot plots represents the abundance of a homo-repeat in (%). The cross marks correspond to the number average of the homo-repeats.

Strikingly, mainly homo-fibrils are observed for the mixture of origami A1 and B1 that possess 0% pattern overlap and only
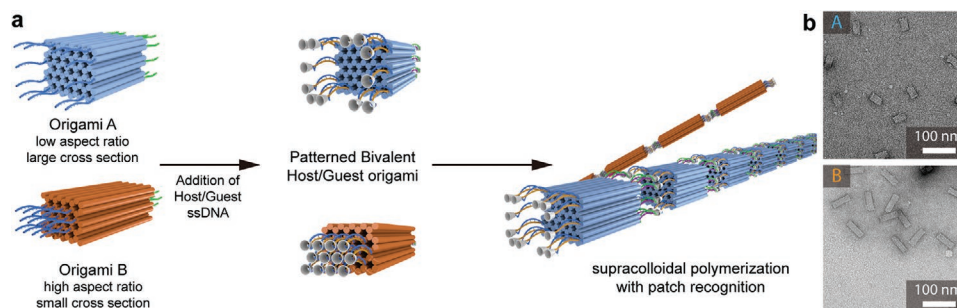

Figure 1. Self-sorting supracolloidal polymerization of 3D DNA origami colloids employing multivalency pattern recognition of host/guest patches. a) Preparation of bivalent Janus colloids with patterns of host/guest units leading to self-sorting SA. b) TEM of both origami.
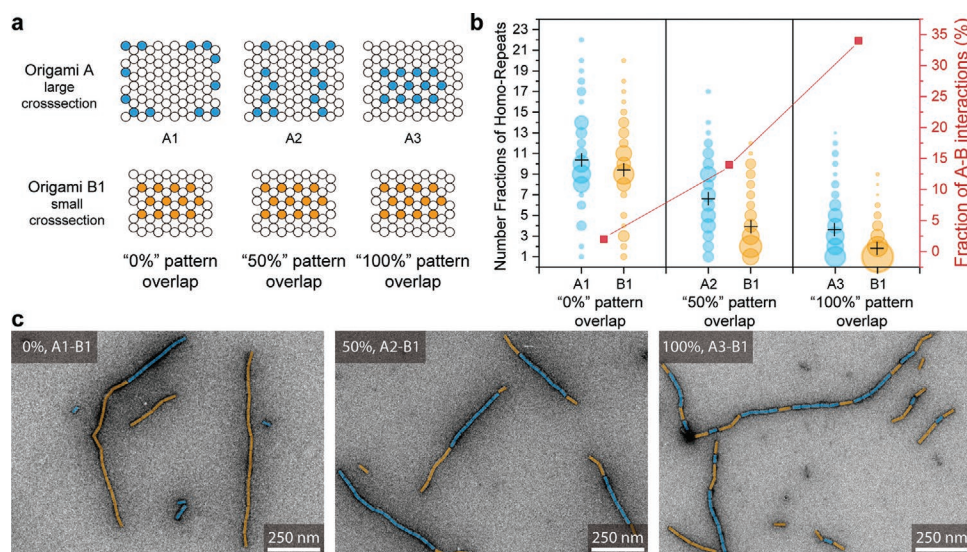
2005668 (2 of 5)

ADVANCED
SCIENCE NEWS
www.advancedsciencenews.com

NANO · MICRO
small
www.small-journal.com

Figure 2. Statistical analysis of supracolloidal co-polymerization with multivalency patterns. a) Multivalency patterns on origami A and B. b) Statistical analysis of the number fraction of homo-repeats in fibrils with a DP > 8, their average degree of polymerization, and the fraction of A–B interactions. c) TEM images of "0%", "50%", and "100%" pattern overlap systems, considering perfectly aligned building blocks.

few crossovers are visible (Figure 2b,c). This confirms highly effective geometric multivalent pattern recognition and a strong preference of each origami towards its own kind. The average length of homo-repeats $X_{n,i}$ for long fibrils with DP > 8 of A1 is 10.5 while the average for B1 is around 9.5 displaying robust polymerization of alike monomers and a low degree of crosstalk. A change from the A1 to the A2 pattern with a theoretical 50% pattern overlap to B1 leads to a significant reduction of both $X_{n,A,B}$ due to increased crosstalk. TEM displays an increasing amount of fibrils containing long homo-repeats of the individual origami. In detail, compared to the A1–B1 system, the decrease of $X_{n,A}$ for this system is less pronounced than for $X_{n,B}$, which indicates a higher affinity of A2–A2 than A1–A1 interactions. We will get back to this below. Systems with fully matched patterns, A3–B1, show that both $X_{n,i}$s are further reduced, generating blocky type co-assembled fibrils with very short homo-repeats ($X_{n,A} = 3.7$; $X_{n,B} = 1.9$) characteristic of a largely statistic integration (Figure 2c).

We also analyzed the fraction of hetero- to homo-interactions for each system. For 0% pattern overlap, the fraction of A–B interactions is as low as 2%, whereas it increases to around 15% for 50% pattern overlap and 35% for a full overlap. However, for a fully statistical interaction of both species, one would expect the fraction of A–B interactions for 100% pattern overlap to be close to 50%. Since the fraction of A–B interactions is only 35% in A3–B1 systems, this indicates that there is still some preference for A3–A3 over A3–B1 interactions albeit having the same pattern.

To better understand this behavior, we performed dimerization experiments of single-tip functionalized origami to estimate the pattern-dependent association rates (K_a) between different patterns.[18] To this end, we prepared stoichiometric solutions of origami pairs with the respective single tip patterns of host or guest units while the other side was passivated by poly-T overhangs (Figures S1 and S2, Supporting Information), and performed a statistical analysis of the dimer

content after 48 h as a function of the origami concentration to estimate K_a (**Table 1**). The K_a of all homo-interactions range from 10^9 to 10^{10} M^{-1}, clearly relying on multivalent binding as compared to the K_a value of a single βCD/Adm interaction of 10^4 M^{-1}.[18] Differences between the patterns are observed, even though all contain the same number of binding units. The A2 pattern shows the highest K_a. The B1–B1 homo interactions of the origami with the smallest cross section are weaker; also smaller compared to A3–A3 having an equivalent pattern. Even though the origin cannot be entirely understood, it may result from differences in general colloidal interactions (electrostatic repulsion, van der Waals attraction and differences in particle diffusion) and different origami shape stiffness. This indicates that subtle changes in the binding patterns and of the interacting patch size are already relevant towards tuning the interaction strengths. Unfortunately, even the largest available ssDNA plasmid (p8064 scaffold) used for the longer origami B does not allow for a similarly sized cross section at longer length needed for distinguishing the origami in TEM.

In contrast, hetero-interactions with less matching patterns show significantly reduced K_a. A1–B1 with the poorest

Table 1. Pattern-dependent association rates K_a of origami patterns during selective dimer formation.

Interaction	Origami	K_a [M^{-1}]
Homo	A1–A1	8.3×10^9
	A2–A2	1.2×10^{10}
	A3–A3	7.1×10^9
	B1–B1	3.6×10^9
Hetero	A1–B1	7.5×10^7
	A2–B1	4.2×10^8
	A3–B1	2.2×10^9
Single βCD/Adm[19]	–	5×10^4

geometric fit has the lowest K_a of $\approx 7.5 \times 10^7$ M^{-1}, A2–B1 with an intermediate overlap features a K_a of 4.3×10^8 M^{-1} and A3–B1 with a perfect overlap features a K_a of $\approx 2.2 \times 10^9$ M^{-1}, which again is on the same order of magnitude as the B1–B1 and A3–A3 interactions. The here shown association rates highly depend on the pattern on the origami, most likely a result of a significant modulation of the underlying effective molarity (EM) of binding partners due to patterning at the patch surface.[6a] In close proximity, a full pattern overlap leads to a large increase of the experienced concentration of binding partners while mismatches lead to less available binding partners and a reduced EM. In summary, a low pattern overlap reduces the hetero K_a constants by two orders of magnitude compared to a perfect fit. This results in negligible hetero-assembly when the patterns are completely unmatched, while for increasing pattern overlap, the K_a constant and resulting crosstalk increase. The extent can be tuned by realizing patterns with a partial overlap. This colloidal K_a interactions manifest on a supracolloidal level in either having statistical blocky structures with increasing blockiness, or even in an almost complete sorting for increasing pattern mismatch.

Building on the understanding developed above, we next designed a scenario, in which the two tips of the origamis were equipped with different patterns of 10 βCD/Adm units. The patterns were designed to maximize hetero-interactions and force a homogeneous co-assembly, while giving minimum possibilities for homo-assembly (**Figure 3**a). In homo-assembly scenarios (only the individual origami, A4 or B2, in solution) only origami A4 can undergo slight homo-fibrillation with a small $X_{n,A}$ of 3.3, whereas origami B2 only forms neglectable assemblies ($X_{n,B} = 1.2$) (Figure 3b; TEM in Figure S3, Supporting Information). This again is in line with the fact that larger cross-section origamis tend to give higher K_a values (cf. Table 1). In stark contrast, for systems containing both origami A4 and B2, the homo-fibrillation of A4 is completely suppressed, and a fraction of 85% hetero-interactions is realized. The corresponding $X_{n,A/B}$s are close to 1, confirming a near perfect alternating co-assembly based on finding the correct front and back side pattern (Figure 3c). In addition, the estimated K_a of A4–A4 is larger than B2–B2 explaining the increased self-assembly preference of A4. Yet in presence of both origami A4 + B2, the desired A4–B2 interactions are the most preferred ones with an almost five times higher K_a than any of the undesired interactions (Figure 3b). Hence, this strategy provides a way to almost reduce the blockiness fully and statistical arrangement (Figure 2c), and forces strict alternating co-assembly.

In summary, we demonstrated self-sorting 3D DNA origami self-assemblies, in which the degree of sorting can be controlled by geometric multivalency pattern recognition on an $\approx 20 \times 20$ nm^2 patch size with controlled overall binding strength. Multivalent binding is observed in all patterns as seen by comparable association rates between same-pattern colloids. Self-sorting is controlled solely through the patterns at the end of the Janus origami modulating the association rates by a factor greater 10^2. Equipping both sides of the same origami with different patterns allows alternating fibril formation with high fidelity.

Our finding of encoding molecular recognition of building blocks by geometric pattern recognition adds a new layer of control towards hierarchical colloidal SA for buildup of orthogonal
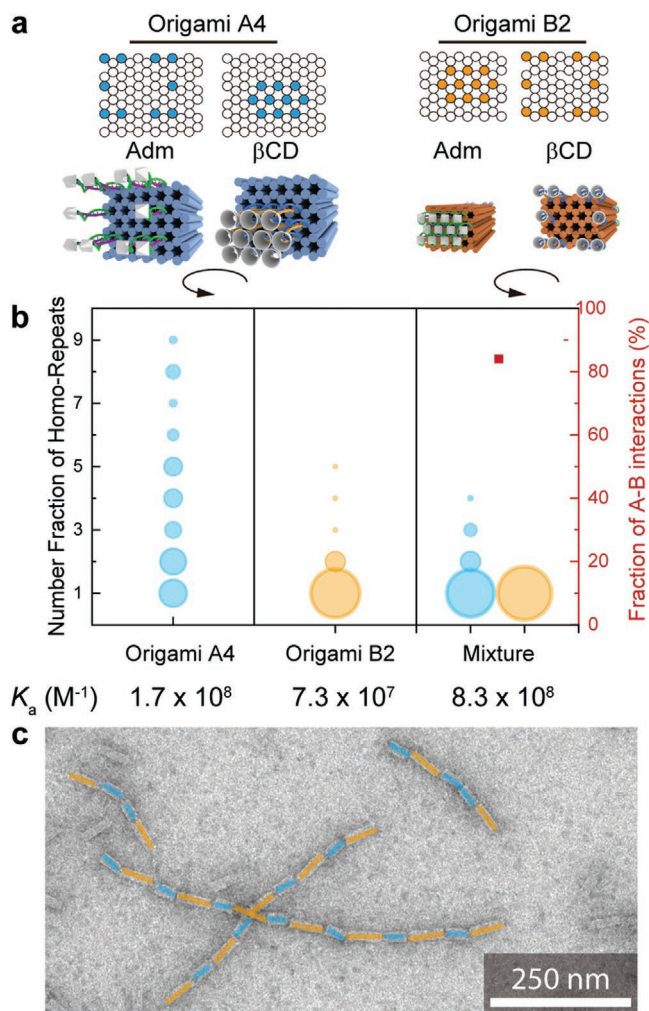

Figure 3. Alternating supracolloidal copolymerization for origami with different patterns at the front and back side. a) Patterns on front and back of the colloids are different from each other yet fitting to the other origami type. b) Number fractions of homo-repeats for DP > 1 for origami A4, B2, and a 1:1 mixture of both origamis. The fraction of A–B interactions over all interactions is greater than 80%. K_a constants determined by selected dimer formation (cf. Figure S4, Supporting Information). c) TEM image of alternating supracolloidal fibrils.

structures. It also underscores that such geometric patterns are not screened due to potential dynamics at the interface and that such rigid DNA origami faces might be very useful for antigen and antibody displays to modulate immunoresponse and other biological interactions, where precise patterns are valuable. We believe that the concept can be extended to engineered proteins for SA, and that the increasing sophistication with which inorganic NPs can be synthesized[19] may also allow for accurately patterning ligands onto other functional NPs to control the organization of functional materials.

Supporting Information

Supporting Information is available from the Wiley Online Library or from the author.

[1] G. M. Whitesides, B. Grzybowski, *Science* **2002**, *295*, 2418.

[2] a) M. Mammen, S.-K. Choi, G. Whitesides, *Angew. Chem., Int. Ed.* **1998**, *37*, 2754; b) M. Waldmann, R. Jirmann, K. Hoelscher, M. Wienke, F. C. Niemeyer, D. Rehders, B. Meyer, *J. Am. Chem. Soc.* **2014**, *136*, 783; c) V. Bandlow, S. Liese, D. Lauster, K. Ludwig, R. R. Netz, A. Herrmann, O. Seitz, *J. Am. Chem. Soc.* **2017**, *139*, 16389.

[3] D. Lauster, S. Klenk, K. Ludwig, S. Nojoumi, S. Behren, L. Adam, M. Stadtmuller, S. Saenger, S. Zimmler, K. Honzke, L. Yao, U. Hoffmann, M. Bardua, A. Hamann, M. Witzenrath, L. E. Sander, T. Wolff, A. C. Hocke, S. Hippenstiel, S. De Carlo, J. Neudecker, K. Osterrieder, N. Budisa, R. R. Netz, C. Bottcher, S. Liese, A. Herrmann, C. P. R. Hackenberger, *Nat. Nanotechnol.* **2020**, *15*, 373.

[4] R. Veneziano, T. J. Moyer, M. B. Stone, E. C. Wamhoff, B. J. Read, S. Mukherjee, T. R. Shepherd, J. Das, W. R. Schief, D. J. Irvine, M. Bathe, *Nat. Nanotechnol.* **2020**, *15*, 716.

[5] S. Woo, P. W. Rothemund, *Nat. Chem.* **2011**, *3*, 620.

[6] a) A. Mulder, J. Huskens, D. N. Reinhoudt, *Org. Biomol. Chem.* **2004**, *2*, 3409; b) O. Crespo-Biel, A. Jukovic, M. Karlsson, D. N. Reinhoudt, J. Huskens, *Isr. J. Chem.* **2005**, *45*, 353; c) R. J. Macfarlane, B. Lee, M. R. Jones, N. Harris, G. C. Schatz, C. A. Mirkin, *Science* **2011**, *334*, 204; d) I. de Feijter, L. Albertazzi, A. R. Palmans, I. K. Voets, *Langmuir* **2015**, *31*, 57; e) J. S. Oh, G. R. Yi, D. J. Pine, *ACS Nano* **2020**, *14*, 4595.

[7] a) E. Elacqua, X. Zheng, C. Shillingford, M. Liu, M. Weck, *Acc. Chem. Res.* **2017**, *50*, 2756; b) W. Li, R. Palis, R. Merindol, J. Majimel, S. Ravaine, E. Duguet, *Chem. Soc. Rev.* **2020**, *49*, 1955.

[8] A. Walther, A. H. Mueller, *Chem. Rev.* **2013**, *113*, 5194.

[9] a) H. Dietz, S. M. Douglas, W. M. Shih, *Science* **2009**, *325*, 725; b) S. M. Douglas, H. Dietz, T. Liedl, B. Hogberg, F. Graf, W. M. Shih, *Nature* **2009**, *459*, 414; c) S. Loescher, S. Groeer, A. Walther, *Angew. Chem., Int. Ed.* **2018**, *57*, 10436.

[10] a) S. Sim, D. Miyajima, T. Niwa, H. Taguchi, T. Aida, *J. Am. Chem. Soc.* **2015**, *137*, 4658; b) A. Schreiber, M. C. Huber, H. Cölfen, S. M. Schiller, *Nat. Commun.* **2015**, *6*, 6705; c) D. Kashiwagi, S. Sim, T. Niwa, H. Taguchi, T. Aida, *J. Am. Chem. Soc.* **2018**, *140*, 26; d) S. E. Geissinger, A. Schreiber, M. C. Huber, L. G. Stuhn, S. M. Schiller, *ACS Synth. Biol.* **2020**, *9*, 827.

[11] a) R. Schreiber, N. Luong, Z. Fan, A. Kuzyk, P. C. Nickels, T. Zhang, D. M. Smith, B. Yurke, W. Kuang, A. O. Govorov, T. Liedl, *Nat. Commun.* **2013**, *4*, 2948; b) A. Kuzyk, R. Schreiber, H. Zhang, A. O. Govorov, T. Liedl, N. Liu, *Nat. Mater.* **2014**, *13*, 862; c) X. Shen, P. Zhan, A. Kuzyk, Q. Liu, A. Asenjo-Garcia, H. Zhang, F. J. de Abajo, A. Govorov, B. Ding, N. Liu, *Nanoscale* **2014**, *6*, 2077.

[12] Z. Zhao, J. Fu, S. Dhakal, A. Johnson-Buck, M. Liu, T. Zhang, N. W. Woodbury, Y. Liu, N. G. Walter, H. Yan, *Nat. Commun.* **2016**, *7*, 10619.

[13] a) J. J. Funke, P. Ketterer, C. Lieleg, S. Schunter, P. Korber, H. Dietz, *Sci. Adv.* **2016**, *2*, e1600974; b) P. C. Nickels, B. Wunsch, P. Holzmeister, W. Bae, L. M. Kneer, D. Grohmann, P. Tinnefeld, T. Liedl, *Science* **2016**, *354*, 305; c) M. W. Hudoba, Y. Luo, A. Zacharias, M. G. Poirier, C. E. Castro, *ACS Nano* **2017**, *11*, 6566.

[14] a) R. Iinuma, Y. Ke, R. Jungmann, T. Schlichthaerle, J. B. Woehrstein, P. Yin, *Science* **2014**, *344*, 65; b) T. Tigges, T. Heuser, R. Tiwari, A. Walther, *Nano Lett.* **2016**, *16*, 7870; c) G. Tikhomirov, P. Petersen, L. Qian, *Nature* **2017**, *552*, 67.

[15] a) T. Gerling, K. F. Wagenbauer, A. M. Neuner, H. Dietz, *Science* **2015**, *347*, 1446; b) K. F. Wagenbauer, C. Sigl, H. Dietz, *Nature* **2017**, *552*, 78; c) W. Pfeifer, P. Lill, C. Gatsogiannis, B. Sacca, *ACS Nano* **2018**, *12*, 44.

[16] S. Loescher, A. Walther, *Angew. Chem., Int. Ed.* **2020**, *59*, 5515.

[17] A. Buchberger, C. R. Simmons, N. E. Fahmi, R. Freeman, N. Stephanopoulos, *J. Am. Chem. Soc.* **2020**, *142*, 1406.

[18] J. Jin, E. G. Baker, C. W. Wood, J. Bath, D. N. Woolfson, A. J. Turberfield, *ACS Nano* **2019**, *13*, 9927.

[19] a) S. Helmi, C. Ziegler, D. J. Kauert, R. Seidel, *Nano Lett.* **2014**, *14*, 6693; b) G. Chen, K. J. Gibson, D. Liu, H. C. Rees, J. H. Lee, W. Xia, R. Lin, H. L. Xin, O. Gang, Y. Weizmann, *Nat. Mater.* **2019**, *18*, 169.

2005668 (5 of 5)